

An innovative approach for the numerical simulation of oil cooling systems

A. Carozza *

Fluid Dynamics Department, CIRA, ITALIAN AEROSPACE RESEARCH CENTRE, Capua, 81043, Italy

(Received April 15, 2014, Revised August 22, 2014, Accepted November 2, 2014)

Abstract. Aeronautics engine cooling is one of the biggest problems that engineers have tried to solve since the beginning of human flight. Systems like radiators should solve this purpose and they have been studied extensively and various solutions have been found to aid the heat dissipation in the engine zone. Special interest has been given to air coolers in order to guide the air flow on engine and lower the high temperatures achieved by the engine in flow conditions. The aircraft companies need faster and faster tools to design their solutions so the development of tools that allow to quickly assess the effectiveness of an cooling system is appreciated. This paper tries to develop a methodology capable of providing such support to companies by means of some application examples. In this work the development of a new methodology for the analysis and the design of oil cooling systems for aerospace applications is presented. The aim is to speed up the simulation of the oil cooling devices in different operative conditions in order to establish the effectiveness and the critical aspects of these devices. Steady turbulent flow simulations are carried out considering the air as ideal-gas with a constant-averaged specific heat. The heat exchanger is simulated using porous media models. The numerical model is first tested on Piaggio P180 considering the pressure losses and temperature increases within the heat exchanger in the several operative data available for this device. In particular, thermal power transferred to cooling air is assumed equal to that nominal of real heat exchanger and the pressure losses are reproduced setting the viscous and internal resistance coefficients of the porous media numerical model. To account for turbulence, the $k-\omega$ SST model is considered with Low-Re correction enabled. Some applications are then shown for this methodology while final results are shown in terms of pressure, temperature contours and streamlines.

Keywords: CFD simulation; aerodynamics; oil cooling; flow field; numerical simulation; porous media

1. Introduction

The present work deals with a new numerical methodology and flow fields analyses of oil cooling duct systems for aerospace applications. This research effort has been conducted in the framework of the European project ESPOSA (Efficient Systems and PrOpulsion for Small Aircraft) of 4th call VII FP, A. Carozza, G. Mingione, (2013), ESPOSA Grant Agreement, PART B: Agreement N 284859. The project develops and integrates novel design and manufacture technologies for a range of small gas turbine engines to provide aircraft manufacturers with modern propulsion units, thus improving efficiency, safety and pilot workload reduction. In

*Corresponding author, Ph.D. Student, E-mail: a.carozza@cira.it



Fig. 1 BE1 pusher aircraft configuration

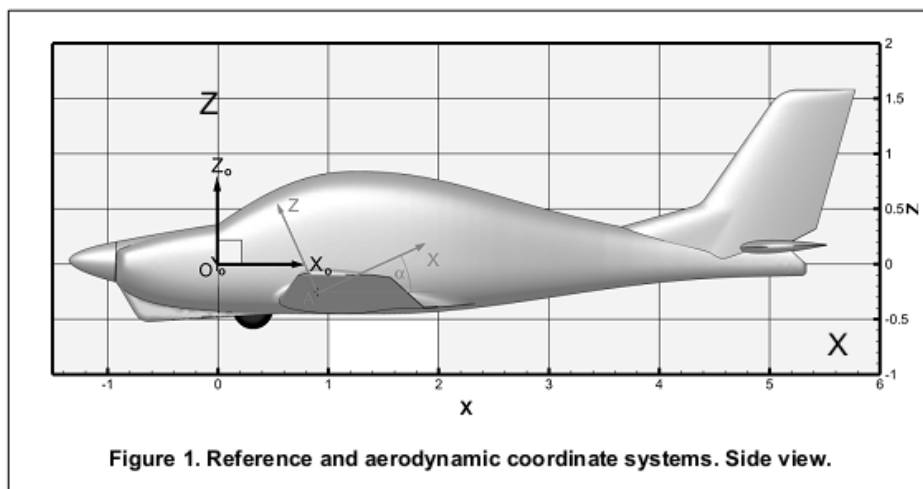


Fig. 2 BE1 tractor aircraft configuration

particular, turbine engine technologies for small aircraft up to 19 seats (under CS-23/FAR23 regulations) operated on the scheduled and non-scheduled flights are investigated. Two engines (Baseline 1 and 2) respectively 160-180 kW and 400-470 kW have been selected and will be installed on four different platforms: tractor configuration with the engine in the fuselage (TR1); tractor configuration with the engine on the wing (TR2); pusher configuration with the engine on the wing (PU2); helicopter configuration (HE1). In this framework CIRA is involved in the engine integration for the configuration PU2 and TR1, shown in Fig. 1 and in Fig. 2, respectively.

To this end computational flow field analyses have been performed to investigate the oil-cooler effectiveness in different critical operative conditions which the airplane experiments in cruise and ground environments because of the lubricating oil should be maintained within certain temperature limits to safeguard the operation of the engine. For instance, due to high manufacturing costs oil cooling design and optimization has recently been resumed after it was widely investigated in the aerospace, ship-building and defense industries. The expanding range of applications is also leading to increased interest in the study of the thermal and transport phenomena in high porosity. This system has the aim of reducing the oil temperature present in the heat exchanger in order to reduce the fuel temperature as well. The commercial code Fluent is used as a solver. In particular, the numerical model used in this work is the porous medium, simulated by means of a negative momentum source. The porous media are widely investigated and

simulated with a number of different numerical models like lattice boltzman methods or finite element methods or simplified correlations methods as in publications (Missirlis *et al.* 2010, Tomimura *et al.* 2004, Hayes *et al.* 2008, Narasimhan *et al.* 2007, Alshare *et al.* 2009, Pavel *et al.* 2004). In this paper, instead, the porous media model has been applied to study and heat exchanger in a duct with the aim of investigating the efficiency of ducts to transport the right air flow rate to lower the oil temperatures and improve the engine efficiency.

Oil coolers are extrapolated from these geometries and right meshed using the grid generator ANSYS ICEM CFD and simulated by means of the commercial code Ansys Fluent 14.5 (2013). Pressure and velocities contours together with other interesting flow field features are reported and studied in this work.

2. Governing equations

The equations governing single-phase flows, the so-called Navier-Stokes equations, have been known for more than a century. Turbulence has a decisive influence on heat transfer, species transport, drag, vorticity distribution, separation and swirl flow. A simplification of the flow equations is obtained when considering an incompressible flow of a Newtonian fluid. The assumption of incompressibility rules out the possibility of sound or shock waves to occur; so this simplification is invalid if these phenomena are important. The incompressible flow assumption typically holds well even when dealing with a “compressible” fluid – such as air at room temperature – at low Mach numbers (even when flowing up to about Mach 0.3). Taking the incompressible flow assumption into account and assuming constant viscosity, the Navier-Stokes equations will read, in vector form

$$\rho \left(\frac{\partial \mathbf{v}}{\partial t} + \mathbf{v} \cdot \nabla \mathbf{v} \right) = -\nabla p + \mu \nabla^2 \mathbf{v} + \mathbf{f} \tag{1}$$

Here \mathbf{f} represents “other” body forces (forces per unit volume), such as gravity or centrifugal force. The shear stress term becomes the useful quantity $\mu \nabla^2 \mathbf{v}$ (∇^2 is the vector Laplacian) when the fluid is assumed incompressible, homogeneous and Newtonian, where μ is the (constant) dynamic viscosity.

It's well worth observing the meaning of each term (compare to the Cauchy momentum equation)

$$\rho \left(\underbrace{\frac{\partial \mathbf{v}}{\partial t}}_{\text{Unsteady acceleration}} + \underbrace{\mathbf{v} \cdot \nabla \mathbf{v}}_{\text{Convective acceleration}} \right) = \underbrace{-\nabla p}_{\text{Pressure gradient}} + \underbrace{\mu \nabla^2 \mathbf{v}}_{\text{Viscosity}} + \underbrace{\mathbf{f}}_{\text{Other body forces}} \tag{2}$$

Note that only the convective terms are nonlinear for incompressible Newtonian flow. The convective acceleration is an acceleration caused by a (possibly steady) change in velocity over position, for example the speeding up of fluid entering a converging nozzle. Though individual fluid particles are being accelerated and thus are under unsteady motion, the flow field (a velocity distribution) will not necessarily be time dependent. Another important observation is that the viscosity is represented by the vector Laplacian of the velocity field (interpreted here as the difference between the velocity at a point and the mean velocity in a small volume around). This implies that – for a Newtonian fluid – viscosity operates in a diffusion of momentum, in much the same way as the diffusion of heat seen in the heat equation (which also involves the Laplacian). If

temperature effects are also neglected, the only “other” equation (apart from initial/boundary conditions) needed is the mass continuity equation. Under the assumption of incompressibility, the density of a fluid parcel is constant and it follows that the continuity equation will simplify to

$$\nabla \cdot \mathbf{v} = 0 \quad (3)$$

This is more specifically a statement of the conservation of volume. These equations are commonly used in 3 coordinates systems: Cartesian, cylindrical, and spherical. While the Cartesian equations seem to follow directly from the vector equation above, the vector form of the Navier–Stokes equation involves some tensor calculus which means that writing it in other coordinate systems is not as simple as doing so for scalar equations. The vector equation written explicitly in Cartesian coordinates is

$$\rho \left(\frac{\partial u}{\partial t} + u \frac{\partial u}{\partial x} + v \frac{\partial u}{\partial y} + w \frac{\partial u}{\partial z} \right) = -\frac{\partial p}{\partial x} + \mu \left(\frac{\partial^2 u}{\partial x^2} + \frac{\partial^2 u}{\partial y^2} + \frac{\partial^2 u}{\partial z^2} \right) + \rho g_x \quad (4)$$

$$\rho \left(\frac{\partial v}{\partial t} + u \frac{\partial v}{\partial x} + v \frac{\partial v}{\partial y} + w \frac{\partial v}{\partial z} \right) = -\frac{\partial p}{\partial y} + \mu \left(\frac{\partial^2 v}{\partial x^2} + \frac{\partial^2 v}{\partial y^2} + \frac{\partial^2 v}{\partial z^2} \right) + \rho g_y \quad (5)$$

$$\rho \left(\frac{\partial w}{\partial t} + u \frac{\partial w}{\partial x} + v \frac{\partial w}{\partial y} + w \frac{\partial w}{\partial z} \right) = -\frac{\partial p}{\partial z} + \mu \left(\frac{\partial^2 w}{\partial x^2} + \frac{\partial^2 w}{\partial y^2} + \frac{\partial^2 w}{\partial z^2} \right) + \rho g_z \quad (6)$$

Note that gravity has been accounted for as a body force, and the values of g_x , g_y , g_z will depend on the orientation of gravity with respect to the chosen set of coordinates. The continuity equation reads

$$\frac{\partial \rho}{\partial t} + \frac{\partial(\rho u)}{\partial x} + \frac{\partial(\rho v)}{\partial y} + \frac{\partial(\rho w)}{\partial z} = 0 \quad (7)$$

When the flow is incompressible, ρ does not change for any fluid parcel, and its material derivative vanishes: $D\rho/Dt = 0$. The continuity equation is reduced to

$$\frac{\partial u}{\partial x} + \frac{\partial v}{\partial y} + \frac{\partial w}{\partial z} = 0 \quad (8)$$

The velocity components (the dependent variables to be solved for) are typically named u , v , w . This system of four equations comprises the most commonly used and studied form. Though comparatively more compact than other representations, this is still a nonlinear system of partial differential equations for which solutions are difficult to obtain. Separation and reattachment of turbulent shear layers can be seen in many practical industrial and engineering applications, either in internal flow systems such as diffusers, combustors and channels with sudden expansion, or in external flows like those past bluff structures and buildings. The RANS equations are used to describe turbulent flows. In this study the SST k - ω two equations turbulence model has been adopted.

2.1 Shear-Stress Transport (SST) k - ω model

The shear-stress transport (SST) k - ω model, Menter (1994), was developed to effectively blend the robust and accurate formulation of the k - ω model in the near-wall region with the free-stream independence of the k - ε model in the far field. To achieve this, the k - ε model is converted into a k - ω formulation. The SST k - ω model is similar to the standard k - ω model, but includes the following refinements:

- The standard $k-\omega$ model and the transformed $k-\varepsilon$ model are both multiplied by a blending function and both models are added together. The blending function is designed to be one in the near-wall region, which activates the standard $k-\omega$ model, and zero away from the surface, which activates the transformed $k-\varepsilon$ model.
- The SST model incorporates a damped cross-diffusion derivative term in the ω equation.
- The definition of the turbulent viscosity is modified to account for the transport of the turbulent shear stress.
- The modeling constants are different.

These features make the SST $k-\omega$ model more accurate and reliable for a wider class of flows than the standard $k-\omega$ model. Other modifications include the addition of a cross-diffusion term in the ω equation and a blending function to ensure that the model equations behave appropriately in both the near-wall and far-field zones.

2.2 Boundary conditions and Numerical procedure

Boundary conditions employed in this study are very classical and simple ones. The hole skin of the model is represented by adiabatic no slip conditions. At the inlet total pressure P_0 and total temperature T_0 are imposed. At the outlet instead ambient pressure and ambient temperature are set. CFD simulations have been carried out following the values indicated in Tables 1-2. When the propeller effect is taken into account, a pressure difference has been added to the total pressure with value of computed by the thrust T divided by the propeller area. When, instead, the fan effect is taken into account, a constant pressure along a face located where the real fan is corresponding to the trade-off working point. A second order scheme has been used to discretize the domain while for the time discretization an implicit scheme has been used. For coupling pressure and velocity a simple projection method has been used. Algebraic multi grid has been used to converge quickly the simulations. In order to ensure a good conversion, 10^4 iterations are performed for each order of discretization. A preliminary study of grid size independence has been done in order to establish what should be the right size and refinement of the grid taking into account both CPU usage and the real available calculation time. Starting with a basic coarse mesh with few hundred thousand cells, the mesh was successfully refined and mass flow rates so achieved are compared as indicated in Table 3. The extrapolation Richardson method has been used to find the reference

Table 1 Boundary conditions for BE1 tractor configuration

Flight test condition	Height [m]	T_0 [K]	P_0 [Pa]	T_s [K]	P_s [Pa]
Cruise	3000.00	274.9	70388	269	70108
Ground	0.00	293.34	102625	288.15	101325
Cruise+ Propeller	3000.00	274.9	73265	269	70108
Ground +Propeller	0.00	293.34	104202	288.15	101325

Table 2 Boundary conditions for BE1 pusher configuration

Flight test condition	Height [m]	T_0 [K]	P_0 [Pa]	T_s [K]	P_s [Pa]
Cruise	2743.2	275.55	72819	270.32	72428.5
Ground+ Fan	0.00	288.15	101325.0	288.15	101325.0

Table 3 Grid independence analysis

Test number	Grid Size [Millions of cells]	Mass flow rate [Kg/s]	Exact Mass flow rate	Error(%)	Number of iterations [$\times 10^3$]
1	0.44	0.075	0.0853	12	5.0
2	0.875	0.08	0.0853	6.2	10.0
3	1.75	0.082	0.0853	4.0	15.0
4	3.5	0.083	0.0853	2.7	20.0

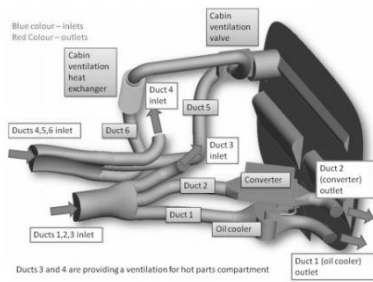


Fig. 3 BE1 tractor ventilation and oil cooling ducts

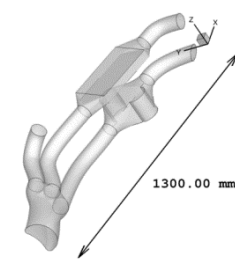


Fig. 4 BE1 tractor oil cooling ducts detail

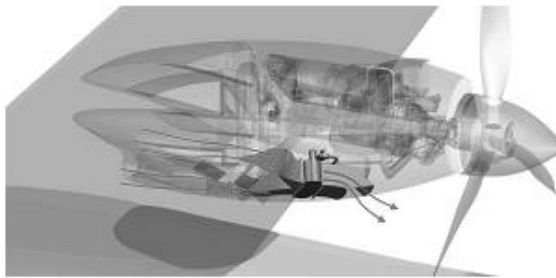


Fig. 5 BE1 pusher oil cooler installation

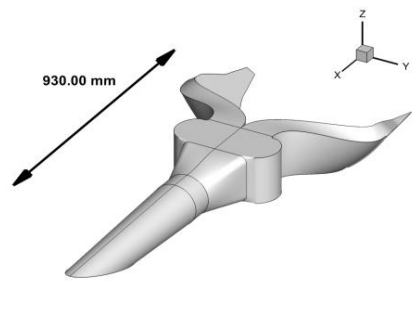


Fig. 6 BE1 pusher oil cooling ducts detail

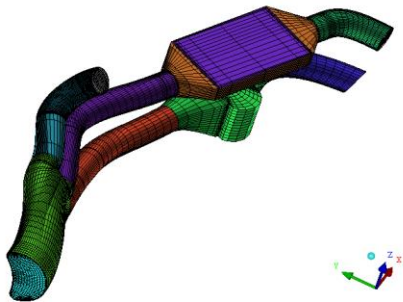


Fig. 7 BE1 tractor oil cooling mesh (coarse level)

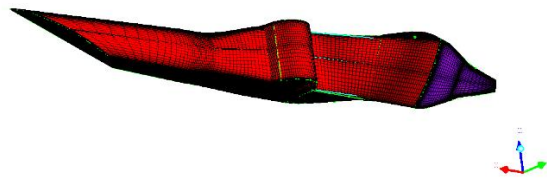


Fig. 8 BE1 pusher oil cooling mesh

value to estimate the error percentage for each grid size. The same mesh settings are used for the other geometries with a small amount of change. The final grid for the case of BE1 tractor consists of about 3.5 million cells, the grid for BE1 pusher is of 0.8 million cells and both grids are used on

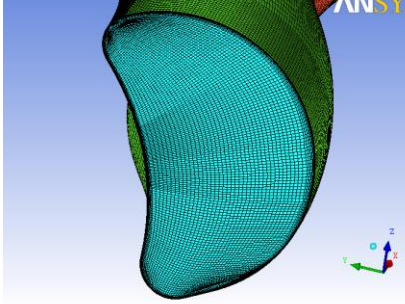


Fig. 9 BE1 tractor oil cooling mesh inlet detail

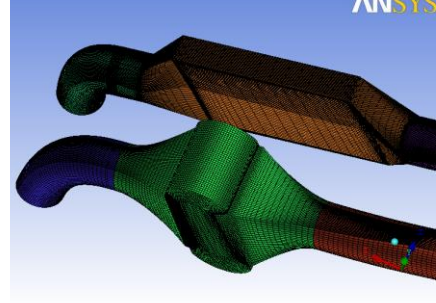


Fig. 10 BE1 tractor mesh density on heat exchanger

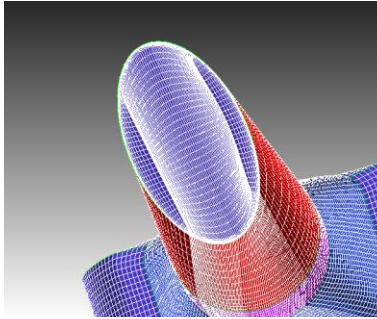


Fig. 11 BE1 pusher oil cooling mesh boundary detail

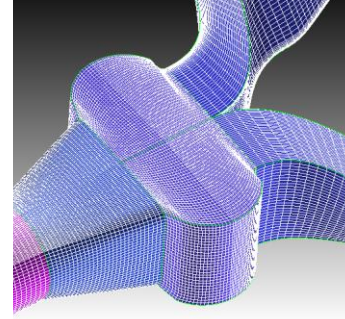


Fig. 12 BE1 pusher oil cooling mesh exchanger detail

16 CPU Linux cluster. Both the grids are of structured kind and are generated taking into account that the SST $k-\omega$ turbulence model requires a good mesh resolution near the wall and an y^+ close to 1 (see Figs. 7-12).

As far as numerical model of oil cooler is concerned, it is worth to note that the heat exchange is schematized as a porous media in thermal equilibrium. Therefore, the heat and pressure losses in the flow are taken into account in the CFD computations by means of source terms in the momentum and energy flow equations, respectively. Momentum source terms in the porous media provides the air pressure drops while thermal source term determines the temperature changing of the air passing through the heat exchanger. The momentum equation reads

$$\frac{\partial}{\partial t}(\rho \vec{v}) + \nabla \cdot (\rho \vec{v} \vec{v}) = -\nabla p + \nabla \cdot (\bar{\tau}) + \rho \vec{g} + \vec{S} \quad (9)$$

where p is the static pressure, $\bar{\tau}$ is the stress tensor, $\rho \vec{g}$ and \vec{S} are the gravitational body force and external body forces, respectively. \vec{S} also contains other model dependent source terms such as porous media. This last term is composed of two parts: a viscous loss and an inertial loss term

$$S_i = -\left(\sum_{j=1}^3 D_{ij} \mu v_i + \sum_{j=1}^3 C_{ij} \frac{1}{2} \rho |v| v_i\right) \quad (10)$$

where S_i is the source term that appears in the i -th (x, y, z) momentum equation, $|v|$ is the magnitude of the velocity. D_{ij} and C_{ij} are matrices called viscous resistance factor and inertial resistance factor. They are defined by the user for specific porous media cases. This momentum sink contributes to the pressure gradient in the porous cell, creating a pressure drop that is proportional to the fluid velocity (or velocity squared) in the cell. In the case of homogeneous

porous media as for oil cooler modeling, Eq. (10) becomes

$$S_i = - \left(\frac{\mu}{\alpha} v_i + C_2 \frac{1}{2} \rho |v| v_i \right) \quad (11)$$

where α is the permeability and C_2 is the inertial resistance factor, simply specify D and C as diagonal matrices with $1/\alpha$ and C_2 on diagonals, respectively. The heat exchanger operative data, provided by manufacturer, allow to extrapolate the air side pressure drop versus velocity and, hence, the determination of viscous resistance ($1/\alpha$) and inertial resistance (C_2) in Eq. (11). Indeed the pressure drop versus flow velocity in the heat exchanger reads

$$\Delta p = av + bv^2 = \left(\frac{\mu}{\alpha} v + \frac{1}{2} C_2 \rho v^2 \right) \Delta n \quad (12)$$

where μ and ρ are evaluated at the operative condition altitude and Δn is the porous media thickness. Therefore, $1/\alpha = a/\mu \Delta n$ and $C_2 = 2b/\rho \Delta n$ determine the momentum source term, see Eq. (10). The a and b coefficients are calculated considering the heat exchanger performances curve and the corresponding regression polynomial curve reported as the one reported in Fig. 13. On the other hand by enabling the energy equation it is possible to make active also a thermal source term in the porous media. FLUENT allows to consider a thermal generation (expressed in W/m^3) in the cell zone corresponding to the heat exchanger. So the porous media thermal generation represents the thermal power transferred to cooling air passing through the heat exchanger. The energy equation for the PM reads

$$\frac{\partial}{\partial t} (\gamma \rho_f E_f + (1 - \gamma) \rho_s E_s) + \nabla \cdot (\vec{v} (\rho_f E_f + p)) = \nabla \cdot [k_{eff} \nabla T - (\sum_i h_i J_i) + (\bar{\tau} \cdot \vec{v})] + S_f^h \quad (13)$$

Where E_f is the total fluid energy, E_s total solid medium energy, γ porosity of the medium, k_{eff} effective thermal conductivity of the medium and S_f^h fluid enthalpy source term. The effective thermal conductivity in the porous medium, k_{eff} , is compared by FLUENT as the volume average of the fluid conductivity and the solid conductivity

$$k_{eff} = \gamma k_f + (1 - \gamma) k_s \quad (14)$$

Where γ is the porosity of the medium, k_f the fluid phase thermal conductivity (including the turbulent contribution) and k_s medium thermal conductivity.

A numerical procedure validation has been carried out taking into account the P180 oil cooler and the experimental available data related to it.

For the P180 geometry, as indicated in equation Eq. (12), viscous and inertial resistances are completed as follows:

Viscous resistance

$$20.598 = \frac{\mu}{\alpha} \Delta n \rightarrow \frac{1}{\alpha} = 5426501.18 \text{ 1/m}^2 \quad (15)$$

Inertial resistance

$$2.1355 = C_2 \frac{1}{2} \rho \Delta n \rightarrow C_2 = 23.10 \text{ 1/m} \quad (16)$$

Observing the curves reported in Fig. 14, it can be said there is a real good agreement between the predicted pressure drops (in red) and the previous experimental values.

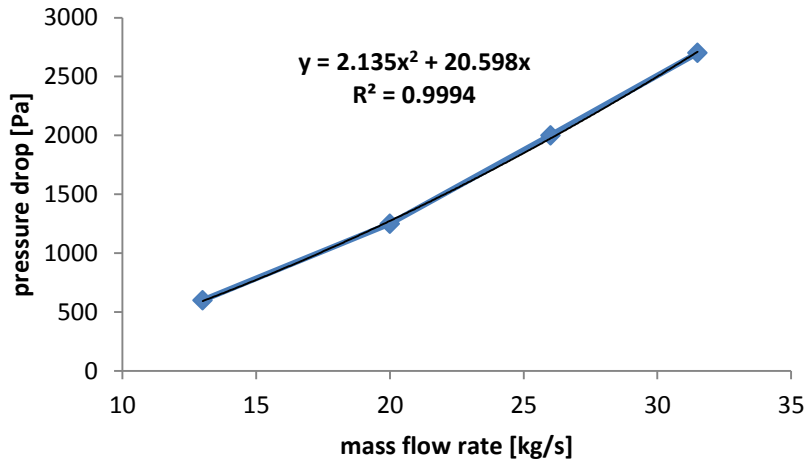


Fig. 13 P180 pressure losses-mass flow rates

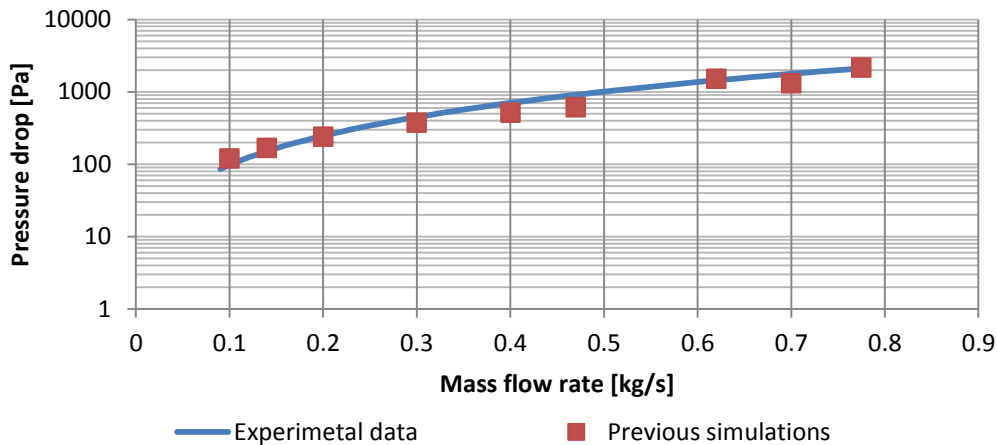


Fig. 14 P180 experimental pressure drop curve and numerical computed value

3. Results and discussion

Oil coolers (and warming systems) are necessary to keep the temperature of the oil, needed for the functioning of the engine and other automotive systems under control. In highly stressed engines the engine oil has to be cooled. Oil cooling can be accomplished by air-cooled heat exchangers or coolant-based oil coolers (i.e., the coolant in the engine cooling circuit). The latter involves simplified oil circuits and lower cost if compared to the oil-air solutions which offer higher performances and do not lead to an additional thermal load for the radiator. Air-cooled oil cooler are generally positioned in the cooling air flow in cars and equipped with an additional fan. Coolant-cooled oil coolers can be incorporated in the coolant tank or engine block, or fitted externally on the engine, transmission, cooling module, or oil filter housing, as required. Oil

Table 4 Target and calculated mass flow rates

Flight test condition	Engine configuration	Mass flow rate(kg/s)	Target mass flow rate(kg/s)
Cruise	Pusher	0.12	0.15
Ground+ Fan	Pusher	0.044	0.02
Cruise	Tractor	0.083	0.15
Cruise+ Propeller	Tractor	0.12	0.15
Ground +Propeller	Tractor	0.0025	0.02

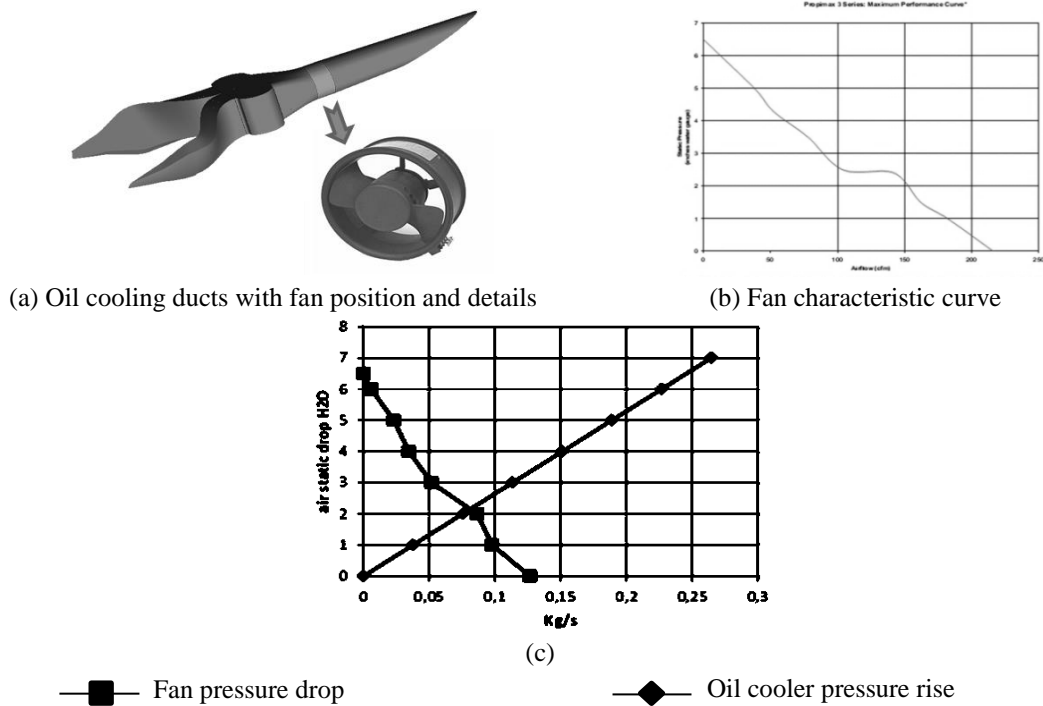


Fig. 15 Trade off graph between fan and unfanned oil cooler pressure drops

coolers are produced in a large variety of designs.

Based on the previous studies and the aforementioned considerations, two different aerospace oil coolers are thermally investigated. Results are provided both in terms of external surface contours and cross section contours. Streamlines are also shown for the whole channel for both the oil coolers in order to investigate the rotational component of the internal flow field. The data collection is subdivided in four test cases:

- Cruise and Ground BE1 tractor
- Cruise and Ground BE1 pusher

Mass flow rates are reported in Table 4.

These results were obtained in a time that does not exceed 24 hours with 4 processors on a cluster with 16 processors. For the design of an oil cooler the above mentioned times are reasonable for simulations that include a numerical model such as porous which typically requires a computational effort greater than the simple case of pure Navier-Stokes equations.

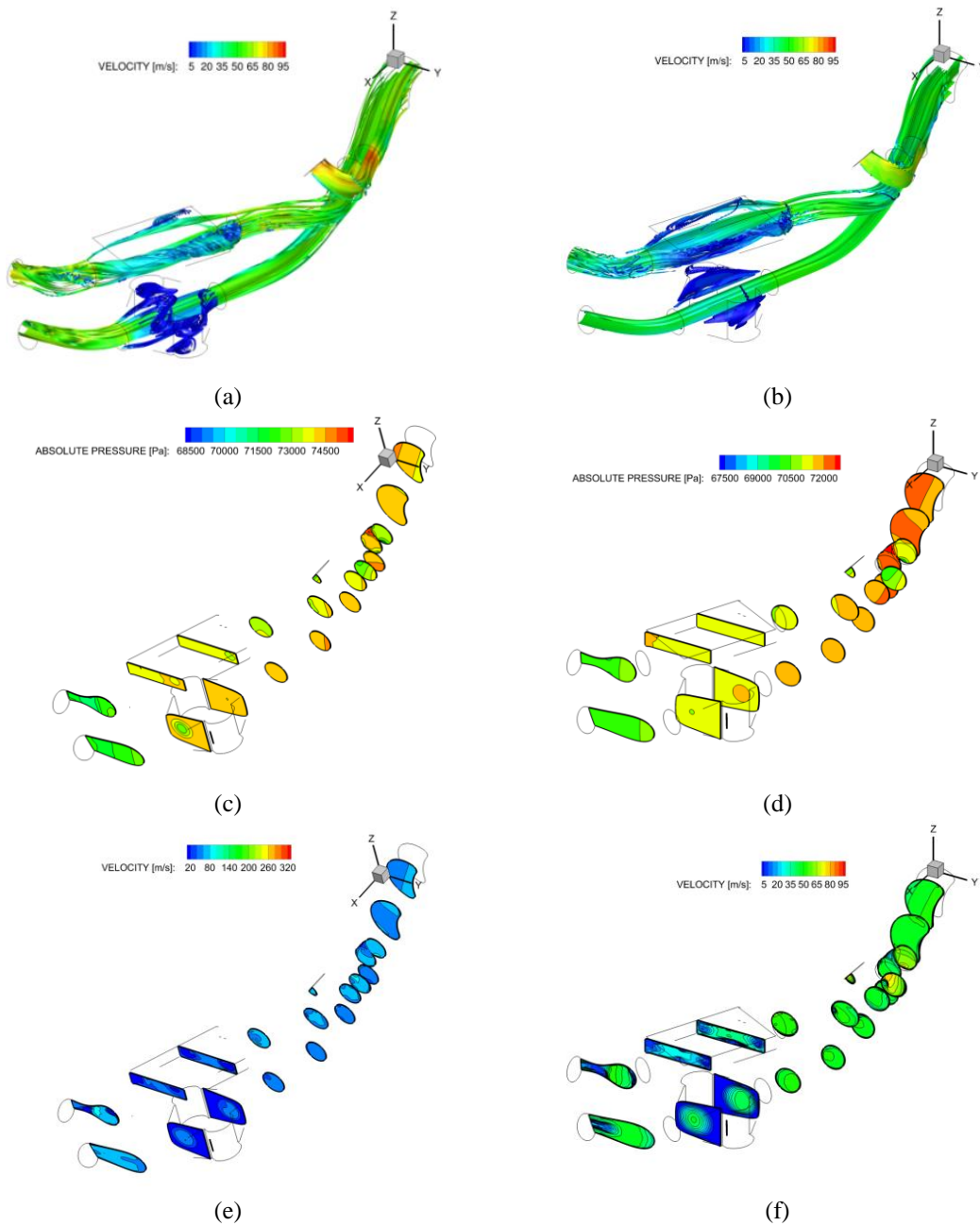


Fig. 16 Streamlines within oil cooling ducts. Left: cruise condition on tractor configuration without propeller, right: cruise condition on tractor configuration with propeller

However, some observations can be done on the two oil coolers under investigation in this paper. For the tractor configuration, looking at numerical results recognized in Fig. 16 and Table 4, one can conclude that cooling air flows quite regularly in the oil cooler ducts. Flow separation is appreciated only in correspondence of heat exchanger, as expected for the effect of the viscous and

inertial resistances of the porous media.

The mass flow rate in cruise condition is slightly lower than the target one (0.15 kg/s), as it can be seen in Table 4. From the Figs. 16(c)-(f), recirculating zones can be noticed in the heat exchanger zone where the velocity achieves quasi zero values and the pressure is just a little over the ambient pressure. On ground the mass flow rate is quite irrelevant with respect to the target one (0.02 kg/s).

For the pusher configuration, instead, the air enters the duct via NACA intakes and flows quite regularly in the whole channel, except in the lower part before the heat exchanger due to the strong twist of the inlet y-shaped ducts.

In Table 4 the mass flow rate in cruise condition is slightly lower than the target one (0.15 kg/s) thanks to the presence of the propeller that increases the momentum source in the ducts. This can be noticed observing the pressure increase at the inlet in Fig. 16(d) or observing the velocity values in Fig. 16(f).

In Figs. 17(b) it can be noticed that the presence of a pressure difference due to the fan effect increases the recirculation inside the outlet ducts and in some manner aids the flow motion. Only the fan presence assures the flow passes through the ducts in ground condition (see Fig. 15(a) where the fan is shown). In this last case the fan performance curve has been crossed with the pressure drop characteristics curve of the unfanned oil cooler. The trade off point shown in Fig. 15(c) has then been used as a working point.

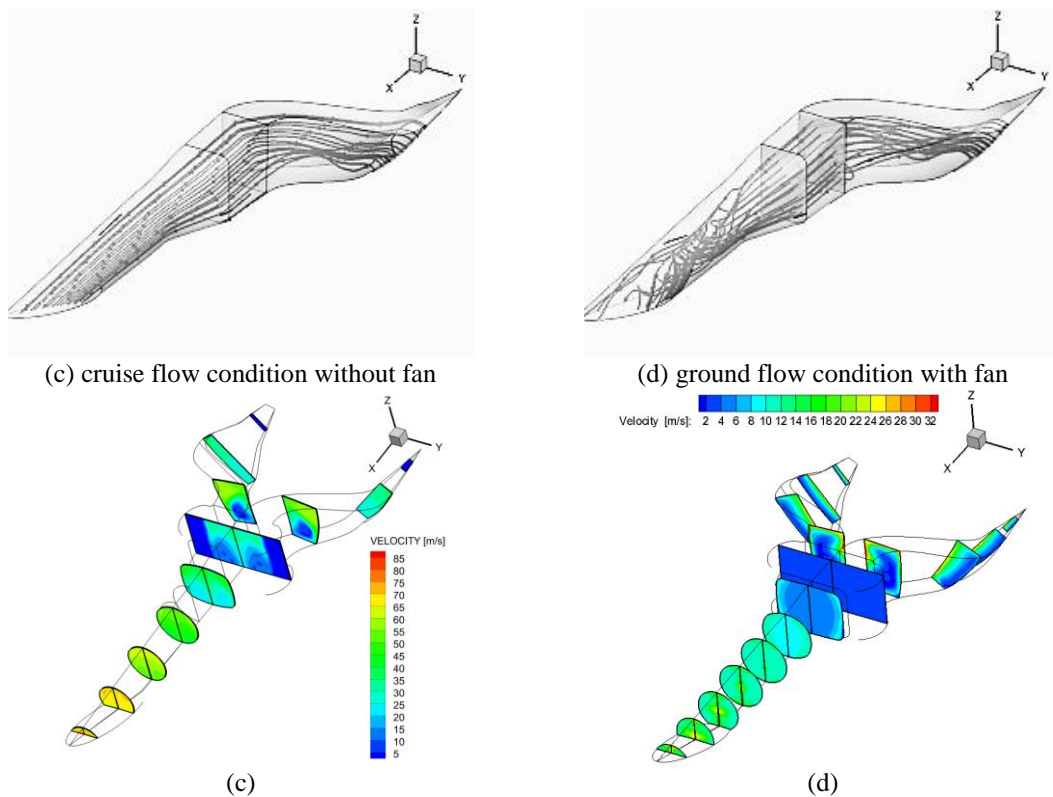


Fig. 17 Streamlines within oil cooling ducts. Left: cruise condition on pusher configuration without fan, right: cruise condition on pusher configuration with fan

4. Conclusions

In this work a flow field simulation of two oil coolers of aeronautical interest has been investigated in the framework of the European Project ESPOSA. Finite volume Navier-Stokes code, namely ANSYS FLUENT 14 and its porous medium numerical model are considered for the CFD simulations. In particular, the porous media model has been considered to simulate the presence of the heat exchanger in the oil cooler device.

Two operative conditions which are cruise and ground flow conditions are numerically investigated. From the observation of the results the following conclusions are derived. The heat source derived by the interaction between the fuel and the oil can speed up the flow and in some manner increase the flow rate; while, on the other hand, the pressure drop in the heat exchanger contributes to lower the mass flow rate value. Further, each oil cooler device is characterized by a cooling air that flows quite regularly. Flow separation occurs only in correspondence of heat exchanger due to the combined effect of viscous and inertial resistances of the porous media model.

From the results so achieved it can be concluded that:

- A good agreement for P180 geometry is achieved between the experiment data and the calculations
- The heat source derived by the interaction between the fuel and the oil can speed up the flow and in some manner increase the flow rate
- The pressure drop in the heat exchanger contributes to lower the mass flow rate value
- Flow separation occurs only in correspondence of heat exchanger due to the combined effect of viscous and inertial resistances of the porous media model

The importance of this work is that a new speedier prediction methodology for the aeronautical oil cooling has been assessed. This methodology can also be applied to other engineering fields like mechanical engineering rather than the heat transfer by air or other working fluids in industrial engineering.

Acknowledgments

This research effort has been funded in the framework of the European project ESPOSA (Efficient Systems and PrOpulsion for Small Aircraft) of 4th call VII FP (ESPOSA Grant Agreement).

References

- Alshare, A.A., Simon, T.W. and Strykowski, P.J. (2009), "Simulations of flow and heat transfer in a serpentine heat exchanger having dispersed resistance with porous-continuum and continuum models", *Int. J. Heat Mass Tran.*, **53**(5), 1088-1099.
- Ansys Fluent 14.5 (2013), Commercially available CFD software package based on the Finite Volume method, User's Guide, A product of Fluent Inc., Centerra Resource Park, 10 Cavendish Court, Lebanon, NH, USA.
- Carozza, A. and Mingione, G. (2013), "Preliminary thermal analysis about BE1 tractor engine components", CIRA-CF-13-022
- Hayes, A.M., Khan, J.A., Shaaban, A.H. and Spearing, I.G. (2008), "The thermal modeling of a matrix heat

- exchanger using a porous medium and the thermal non-equilibrium model”, *Int. J. Therm. Sci.*, **47**(10), 1306-1315.
- Menter, F.R. (1994), “Two-equation Eddy-Viscosity turbulence models for engineering applications”, *AIAA J.*, **32**(8), 1598-1605.
- Missirlis, D., Yakinthos, K., Palikaras, A., Katheder, K. and Goulas, A. (2005), “Experimental and numerical investigation of the flow field through a heat exchanger for aero-engine applications”, *Int. J. Heat Fluid Flow*, **26**(3), 440-458..
- Missirlis, D., Donnerhack, S., Seite, O., Albanakis, C., Sideridis, C., Yakinthos, K. and Goulas, A. (2010), “Numerical development of a heat transfer and pressure drop porosity model for a heat exchanger for aero engine applications”, *Appl. Therm. Eng.*, **30**(11), 1341-1350.
- Narasimhan, A. and Sumuthra Raju, K.S. (2007), “Effect of variable permeability porous medium inter-connectors on the thermo-hydraulics of heat exchanger modeled as porous media”, *Int. J. Heat Mass Tran.*, **50**(19), 4052-4062.
- Pavel, B.I. and Mohamad, A.A. (2004), “An experimental and numerical study on heat transfer enhancement for gas heat exchangers fitted with porous media”, *Int. J. Heat Mass Tran.*, **47**(23), 4939-4952.
- Tomimura, T., Hamano, K., Honda, Y. and Echigo, R. (2004), “Experimental study on multi-layered type of gas-to-gas heat exchanger using porous media”, *Int. J. Heat Mass Tran.*, **47**(21), 4615-4623.